JACS
JOURNAL OF THE AMERICAN CHEMICAL SOCIETY
Article
pubs.acs.org/JACS

Influence of Charge and Coordination Number on Bond Dissociation Energies, Distances, and Vibrational Frequencies for the Phosphorus−Phosphorus Bond

Saurabh S. Chitnis,[†,‡] J. Marc Whalen,[‡] and Neil Burford*[,†,‡]

[†]Department of Chemistry, University of Victoria, Victoria, British Columbia V8W 3V6, Canada
[‡]Department of Chemistry, Dalhousie University, Halifax, Nova Scotia B3H 4J3, Canada

Supporting Information

ABSTRACT: We report a comprehensive and systematic experimental and computational assessment of the P−P bond in prototypical molecules that represent a rare series of known compounds. The data presented complement the existing solid-state structural data and previous computational studies to provide a thorough thermodynamic and electronic understanding of the P−P bond. Comparison of homolytic and heterolytic bond dissociation for tricoordinate-tricoordinate, tricoordinate-tetracoordinate, and tetracoordinate-tetracoordinate P−P bonds in frameworks **1**−**6** provides fundamental insights into covalent bonding. For all types of P−P bond discussed, homolytic dissociation is favored over heterolytic dissociation, although the distinction is small for $\mathbf{2}^{1+}$ and $\mathbf{6}^{1+}$. The presence of a single cationic charge in a molecule substantially strengthens the P−P bond (relative to analogous neutral frameworks) such that it is comparable with the C−C bond in alkanes. Nevertheless, P−P distances are remarkably independent of molecular charge or coordination number, and trends in values of d(PC) and ν_{symm}(PC) imply that a molecular cationic charge is distributed over the alkyl substituents. In the gas phase, the diphosphonium dication $\mathbf{3}^{2+}$ has similar energy to two $[PMe_3]^+$ radical cations, so that it is the lattice enthalpy of $\mathbf{3}[OTf]_2$ in the solid-state that enables isolation, highlighting that values from gas-phase calculations are poor guides for synthetic planning for ionic compounds. There are no relationships or correlations between bond lengths, strengths, and vibrational frequencies.

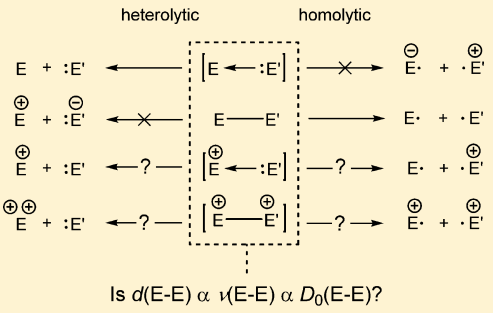

INTRODUCTION

The strength of a covalent bond (E−E′) is an important characteristic that determines the reactivity of a molecule and provides insight into the electronic structure. Energies for homolytic and heterolytic dissociation for a given bond can be substantially different. For instance, the S−B bond in Me_2SBH_3 is observed to undergo facile heterolytic dissociation to give Me_2S and BH_3 (Chart 1, Case I, E = B, E′ = S), while homolytic dissociation into a dimethylsulfide radical cation and borane radical anion is not observed because, in the gas phase, the electron affinity of BH_3 (0.038 ± 0.015 eV)[1] is much less than the ionization energy of Me_2S (8.706 ± 0.010 eV).[2]

Chart 1. Homolytic and Heterolytic Dissociation Pathways for an E−E′ Bond

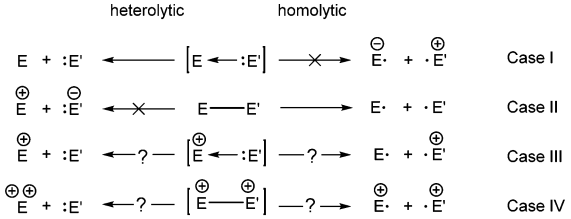

Consequently, the S−B bond is described as a "coordinate bond" (or "dative bond"), sometimes illustrated using the arrow notation, $Me_2S \rightarrow BH_3$. In contrast, heterolytic dissociation of a bond that requires separation of oppositely charged fragments, such as the C−C bond in ethane, is intuitively energetically more costly than homolytic dissociation (Chart 1, Case II, E = E′ = C). As a result, when referring to such examples, usage of the term "bond strength" in compounds representing Case I and Case II implicitly denotes the energy required for heterolytic and homolytic dissociation, respectively.[3−5] In comparison, the thermodynamic difference between homolytic or heterolytic dissociation is less obvious for bonds in charged molecules (Cases III and IV).

The P−P bonded frameworks **1**−**6** (Chart 2) represent a rare series of known compounds that offer the opportunity to assess the energetic preferences for cases II, III, and IV by sampling possible combinations of tricoordinate and tetracoordinate phosphorus centers with varying charge and coordination number. The structure of tetramethyldiphosphine (**1**) is well established in the solid state[6] and the gas phase.[7] The pentamethylphosphinophosphonium cation ($\mathbf{2}^{1+}$) as chloride[8]

Received: July 21, 2014
Published: August 8, 2014

   dx.doi.org/10.1021/ja507413s | J. Am. Chem. Soc. 2014, 136, 12498−12506

Chart 2. Prototypical Tricoordinate and Tetracoordinate P−P Bonded Frameworks

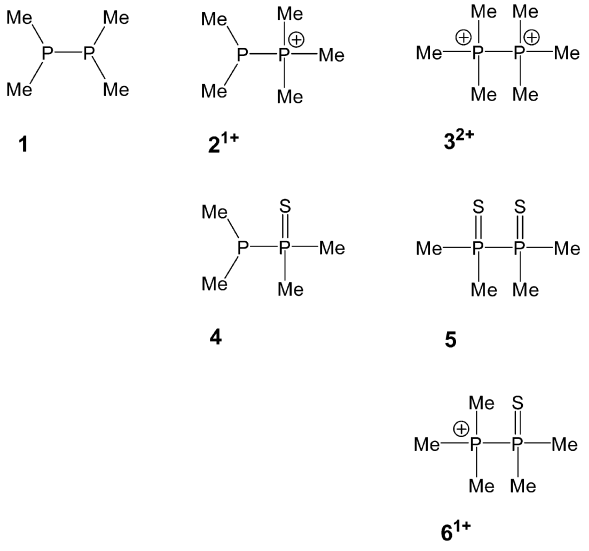

and triflate (OTf = OSO_2CF_3)[9] salts, the bis-triflate salt of the hexamethyldiphosphonium cation ($\mathbf{3}^{2+}$),[9] tetramethyldiphosphine sulfide (**4**),[10] tetramethyldiphosphine disulfide (**5**),[11] and the triflate salt of the pentamethylphosphoniumphosphine sulfide cation ($\mathbf{6}^{1+}$)[12] have also been structurally characterized in the solid state.

The experimental data for P−P bond dissociation energies in frameworks **1**−**6** are intuitively inconsistent. For **1**, a homolytic dissociation energy of 440 kJ mol^{-1} was indirectly obtained from the difference in the mass-spectral appearance potentials of the $[Me_2P]^{1+}$ and $[Me_2PPMe_2]^{1+}$ ions[13] and is suspiciously high given that calculated values lie in the 220−260 kJ mol^{-1} range.[14] For cations of the form $[R_2P\text{-}PMe_3]^{1+}$ ($\mathbf{2}^{1+}$ is a prototypical case), a gas-phase computational study concluded that heterolytic P−P bond dissociation to give $[R_2P]^{1+}$ and PMe_3 was preferred by ca. 130 kJ mol^{-1} when R is a π-donating substituent (R = Me_2N), and homolytic dissociation to give Me_2P and $[PMe_3]^{1+}$ was preferred by ca. 30 kJ mol^{-1} when R is a σ-donating substituent (R = Me).[15] An atoms-in-molecules (AIM) investigation concluded that the P−P bond energies calculated from electron densities at bond critical points increased in the order: **1**(183 kJ mol^{-1}) < $\mathbf{2}^{1+}$ (188 kJ mol^{-1}) < $\mathbf{3}^{2+}$ (190 kJ mol^{-1}).[16]

We now provide a comprehensive experimental and computational assessment of the P−P bond that complements the reported solid-state structural data and previous computational studies. A systematic computational analysis of homolytic versus heterolytic P−P bond dissociation in frameworks **1**−**6** is supported by vibrational analysis with unambiguous assignment of the P−E (E = P, C) frequencies using isotopic enrichment techniques. The variations in solid-state structural parameters, computed dissociation energies, and stretching frequencies as a function of the overall charge on the compound and the coordination number of each phosphorus center provides important insights and a more definitive understanding of the P−P bond. It is possible that the findings described for P−P bonds will be applicable to other homoatomic bonds.

RESULTS AND DISCUSSION

Calculated P−P Bond Energies. The Gibbs energies and enthalpies of various P−P bond dissociation processes were calculated at the MP2/cc-pVTZ level at 298 K for frameworks **1**−**6** in the gas phase (Scheme 1).[17] The trends in bond enthalpy are closely reflected in the Gibbs energies. The heterolytic dissociation enthalpy of **1** into $[PMe_2]^+$ and $[PMe_2]^-$ is 735 kJ mol^{-1} more than homolytic dissociation into two PMe_2 radicals, and a similar distinction is expected for ethane. In contrast, for $\mathbf{2}^{1+}$, heterolytic dissociation is only 15 kJ

Scheme 1. Reaction Gibbs Energies (kJ mol^{-1}, above arrow) and Enthalpies (kJ mol^{-1}, below arrow) for the P−P Bond Dissociation in Frameworks 1−6[a]

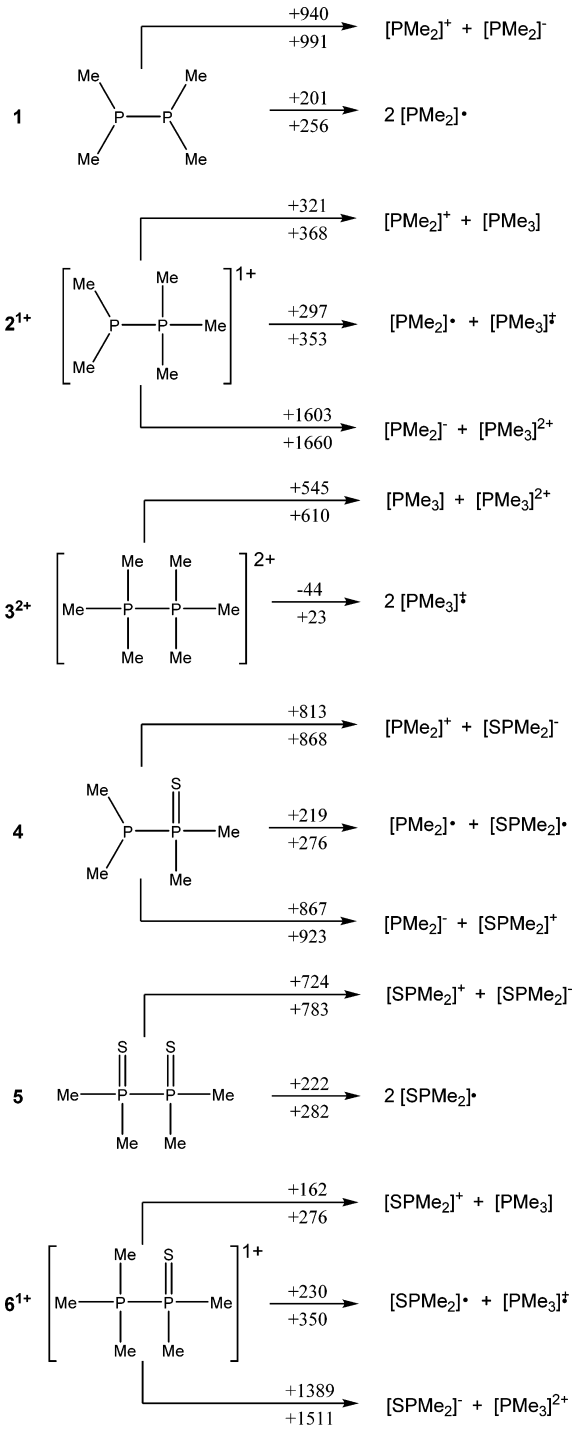

[a]All species were modelled in the gas phase at 298 K at the MP2/cc-pVTZ level.

dx.doi.org/10.1021/ja507413s | J. Am. Chem. Soc. 2014, 136, 12498−12506

mol^{-1} greater than homolytic dissociation. Moreover, the homolytic dissociation of $\mathbf{2}^{1+}$ is substantially greater than homolytic dissociation of all other frameworks considered except the phosphoniumphosphine sulfide cation, $\mathbf{6}^{1+}$. The homolytic and heterolytic P−P dissociations of **5** have enthalpies that are similar to those of **1**, and the former pathway is preferred in both compounds. For **1**, these observations are consistent with its reactivity toward unsaturated systems, for example 1,3-butadiene, which results in the formation of the homolytic P−P cleavage product 1,4-bis(dimethylphosphino)-but-2-ene.[18] Heterolytic dissociation of the P−P bond appears to be prohibitively endothermic in all cases except $\mathbf{2}^{1+}$, $\mathbf{3}^{2+}$, and $\mathbf{6}^{1+}$ in which P−P dissociation can occur without separation of oppositely charged ions. The relatively small heterolytic dissociation energy for $\mathbf{2}^{1+}$ and $\mathbf{6}^{1+}$ predicts that these cations may undergo displacement of the PMe_3 group by a stronger donor such as an N-heterocyclic carbene (NHC) to give the corresponding $[NHC\text{-}P(S)Me_2]^{1+}$ cations, a derivative of which has been prepared via a different synthetic route.[19]

Introduction of Me^+ to **1** to give $\mathbf{2}^{1+}$ effects an increase in the homolytic P−P bond enthalpy of 97 kJ mol^{-1}, and the value for $\mathbf{2}^{1+}$ (353 kJ mol^{-1}) is of the order of the corresponding C−C bond dissociation enthalpy in simple alkanes such as ethane (377 ± 1 kJ mol^{-1}).[20] This result illustrates the energetic consequences of the isolobality between alkanes and phosphonium cations, a feature that has enabled the isolation of a diverse family of cationic *catena*-phosphorus compounds representing phosphorus analogues of hydrocarbon frameworks.[21,22] In this context, it is interesting to note (Figure 1)

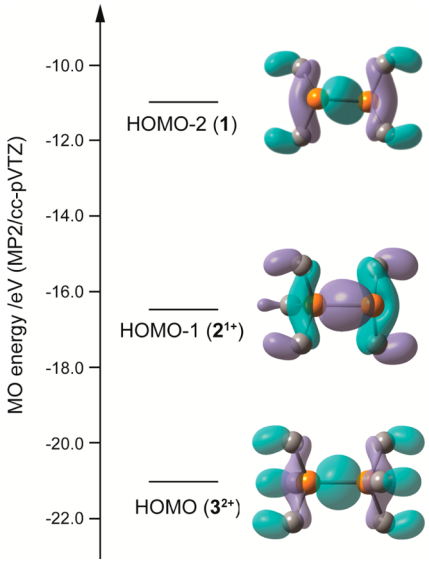

Figure 1. Calculated (MP2/cc-pVTZ) energies and isosurfaces (isovalue = 0.05) for the principal P−P σ-bonding orbital in **1**, $\mathbf{2}^{1+}$, and $\mathbf{3}^{2+}$. Hydrogen atoms are not shown for clarity.

that the energy of the dominant P−P σ-bonding MO shows the trend: **1** (−11.0 eV) > $\mathbf{2}^{1+}$ (−16.4 eV) > $\mathbf{3}^{2+}$ (−21.1 eV). Implication of a substantially stronger P−P bond in $\mathbf{2}^{1+}$ is consistent with the relative homolytic bond enthalpies of **1** and $\mathbf{2}^{1+}$, but the relatively low energy of the primary P−P σ-bonding MO in $\mathbf{3}^{2+}$ is inconsistent with calculated metastability of this cation in the gas phase with respect to dissociation into two $[PMe_3]^+$ radical cations (ΔG_{rxn} = −44 kJ mol^{-1}, ΔH_{rxn} = +23 kJ mol^{-1}). We infer that in the gas phase, frameworks involving one or two tetracoordinate centers adopt a relatively strong P−P bond, except in the case of $\mathbf{3}^{2+}$ (*vide infra*), where the stabilizing influence of introducing cationic charge is constrained by Coulombic destabilization due to charge concentration. Therefore, successful isolation of polycations such as $\mathbf{3}^{2+}$ depends upon the choice of anions and solid-state thermodynamics.[23] Enhancement by approximately 70 kJ mol^{-1} of the P−P homolytic bond enthalpy due to the presence of a single cationic charge is also evidenced by comparison of the P−P dissociation enthalpies of $\mathbf{2}^{1+}$ (353 kJ mol^{-1}) and **4** (276 kJ mol^{-1}) as well as comparison of $\mathbf{6}^{1+}$ (350 kJ mol^{-1}) and **5** (282 kJ mol^{-1}).

Despite the facility of homolytic P−P dissociation in $\mathbf{3}^{2+}$, a stable bis-triflate salt of $\mathbf{3}^{2+}$ has been obtained via three distinct reactions (Scheme 2): (i) methylation of **2**[OTf],[9] (ii) nucleophilic displacement of 4-dimethylaminopyridine (DMAP) by PMe_3 from $[Me_3P(DMAP)][OTf]_2$,[24] and (iii) reductive elimination from $[Sb(PMe_3)_3][OTf]_3$[25] or from $[Ph_3Sb(PMe_3)_2][OTf]_2$.[26] We attribute the formation of $\mathbf{3}[OTf]_2$ in these reactions to the lattice enthalpy expected for an MX_2 salt and have determined Born−Haber−Fajans cycles for the thermodynamically favored stepwise methylation of **1** to give **2**[OTf] and $\mathbf{3}[OTf]_2$ (Scheme 3).

The lattice enthalpies of the salts of **2**[OTf] and $\mathbf{3}[OTf]_2$ in Scheme 3 were estimated using the volume-based thermodynamics (VBT) approach (see Supporting Information for details).[27] The volume of $\mathbf{3}[OTf]_2$ was obtained from its crystal structure.[16] Since the solid-state structure of **2**[OTf] is not known, the volume of **2** was obtained from **2**[Cl] and added to an average volume for the triflate anion observed in several M[OTf] salts (M = Li, Na, K, NH_4).[28] The enthalpies of vaporization for MeOTf and **1** were derived from Trouton's rule using experimentally known boiling points. The most reliable gas-phase enthalpy of dissociation for MeOTf into $[Me]^{1+}$ and $[OTf]^{1-}$ has been reported using calculations at the MP2/aug-cc-pVnZ (n = D, T, Q) level, extrapolated to the complete basis-set (CBS) limit.[28] The P−C bond dissociation enthalpies were calculated at the MP2/cc-pVTZ level.

The P−C bond resulting from the methylation of **2**[OTf] is much weaker (177 kJ mol^{-1}) than that resulting from the first methylation (621 kJ mol^{-1}) and the large difference between the two values evidence the greater Lewis basicity of neutral **1** compared to cationic $\mathbf{2}^{1+}$. Nevertheless, the relatively large lattice enthalpy of $\mathbf{3}[OTf]_2$ (1432 kJ mol^{-1}) is sufficient to make methylation of **2**[OTf] thermodynamically favored. A similar analysis is carried out in Scheme 4 for nucleophilic displacement of DMAP by PMe_3 from $[Me_3P(DMAP)][OTf]_2$.[24] The sublimation enthalpy of DMAP was obtained as a sum of its reported enthalpy of fusion[29] and calculated (Trouton's rule using experimental boiling point)[30] enthalpy of vaporization. Thermochemical analyses of the two reductive elimination pathways (Scheme 2, (iii)) are precluded by the unknown sublimation enthalpies for the solids.

Scheme 5 shows thermochemical cycles for the decomposition of $\mathbf{3}[OTf]_2$ in the solid state to give free PMe_3 and $[PMe_3][OTf]_2$ (heterolytic P−P dissociation) or to give 2 equivalents of $[PMe_3][OTf]$ (homolytic P−P dissociation). To estimate the lattice enthalpy of $[PMe_3][OTf]_2$, the volume of the $[PMe_3]^{2+}$ was approximated as 50% of the volume of the $[Me_3PPMe_3]^{2+}$ ion and represents a conservative estimate rather than an accurate value. Nevertheless, due to the large endothermic term arising from heterolytic dissociation of $\mathbf{3}^{2+}$ in

dx.doi.org/10.1021/ja507413s | J. Am. Chem. Soc. 2014, 136, 12498−12506

Scheme 2. Three Experimental Routes to $3[OTf]_2$: (i) Methylation, (ii) Nucleophilic Displacement, and (iii) Reductive Elimination

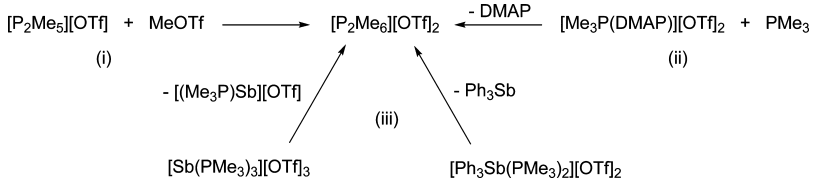

Scheme 3. Born–Haber–Fajans Cycles for the Formation of $2[OTf]$ (left) and $3[OTf]_2$ (right) via Stepwise Methylation of 1[a]

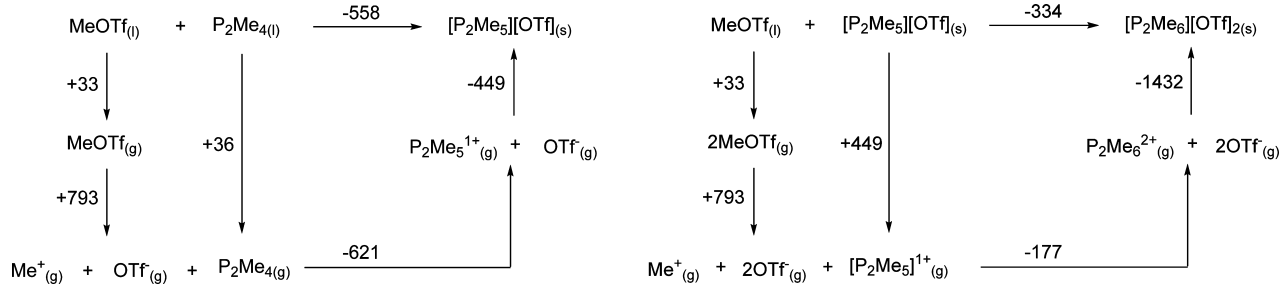

[a]All enthalpy values are in kJ mol^{-1}.

Scheme 4. Born–Haber–Fajans Cycle for the Formation of $3[OTf]_2$ from Nucleophilic Displacement of DMAP from $[Me_3P(DMAP)][OTf]_2$[a]

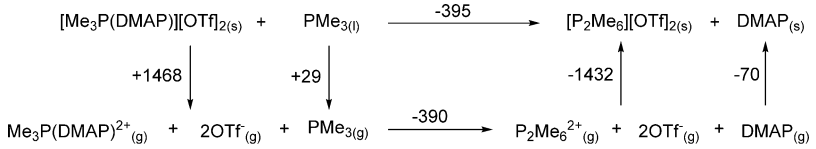

[a]All enthalpy values are in kJ mol^{-1}.

Scheme 5. Born–Haber–Fajans Cycles for the Heterolytic (left) and Homolytic (right) Dissociation of $3[OTf]_2$ in the Solid State[a]

[a]All values are in kJ mol^{-1}.

the gas phase, the error in this volume can be as large as 50% while still yielding a 200 kJ mol^{-1} barrier to the overall decomposition. The volume of the $[PMe_3]^{1+}$ radical cation was calculated as 40% of the known volume of PMe_3 based on the experimental observation that there is a 24–44% contraction of volume going from an PR_3 to $[PR_3]^{1+}$ radical cation in the two cases where such crystallographic data exist.[31,32] Thus, the 40% volume contraction estimated here provides an upper limit for the lattice enthalpy of $[PMe_3][OTf]$. The results indicate that $3[OTf]_2$ is thermodynamically stable in the solid state with respect to P–P dissociation, despite the ease of P–P dissociation of gaseous 3^{2+}.

The similarity of the enthalpy for homolytic (+447 kJ mol^{-1}) and heterolytic (+490 kJ mol^{-1}) P–P bond dissociation (Δ = 43 kJ mol^{-1}) in the solid state suggests that solutions of $3[OTf]_2$ may exhibit reactivity consistent with both dissociation modes depending upon the reaction conditions. Although these experiments have not been reported, a reactivity study[33] of the closely related salt, hexapropyldiphosphonium diperchlorate, $[P_2Pr_6][ClO_4]_2$, showed reaction with dipropyldisulfide (PrS-SPr) to yield $[Pr_3P\text{-}SPr][ClO_4]$, implicating homolytic P–P and S–S dissociation. In addition, solutions of $[P_2Pr_6][ClO_4]_2$ react with fluoride in $[Et_4N][F]$ to yield Pr_3PF_2 and free Pr_3P, indicative of heterolytic P–P bond dissociation.

Vibrational Spectroscopy. Figure 2 shows the room-temperature infrared spectra of **1** (neat liquid), **2**[OTf] (Nujol mull) and $3[OTf]_2$ (Nujol mull), together with the low-temperature (−75 °C) Raman spectra of powdered **1**, **2**[OTf], and $3[OTf]_2$. A complete list of frequencies is given in the Supporting Information. While the P–P stretching mode (ca. 450 cm^{-1}) is infrared-silent in **1** and $3[OTf]_2$ and weak in **2**[OTf], it is Raman active and intense in all cases. At room temperature, **1** exists as an equilibrium mixture of *trans* (C_{2h}) and *gauche* (C_2) conformers in a 60:40 ratio.[34] Upon cooling to −75 °C, only the *trans* isomer is observed in the Raman spectrum of solid **1**. The presence of an inversion center in 3^{2+} is responsible for mutual exclusion of peaks between the infrared and Raman modes for the dication. In Figure 2, 14

dx.doi.org/10.1021/ja507413s | J. Am. Chem. Soc. 2014, 136, 12498–12506

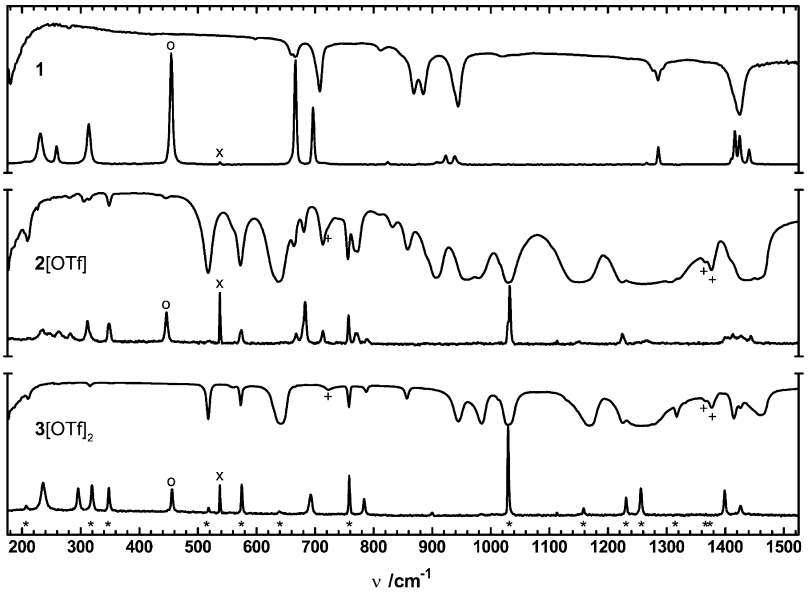

Figure 2. Raman (bottom, −75 °C, Pyrex tube, 1064 nm excitation) and infrared (top, 25 °C, CsI plates) spectra of **1**, **2**[OTf], and **3**$[OTf]_2$. The infrared spectrum of **1** was obtained on a neat liquid sample, while the infrared spectra of **2**[OTf] and **3**$[OTf]_2$ were obtained for samples prepared as Nujol mulls. The Raman spectra were obtained for solid samples. Symbols denote anion modes (*), the P−P stretching mode (o), Nujol modes (+), and an instrumental artifact (x).

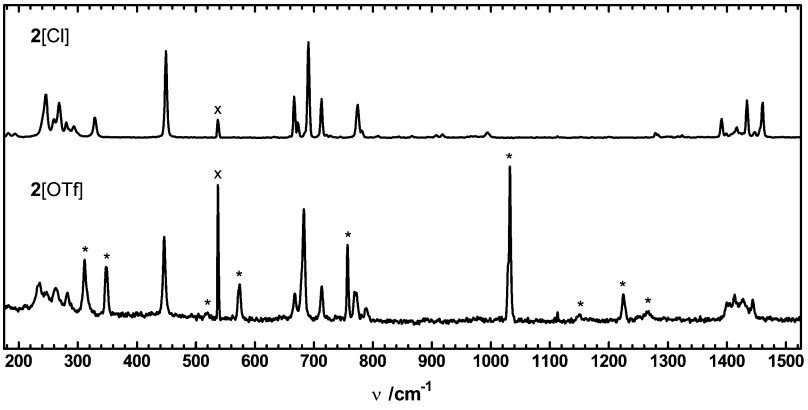

Figure 3. Raman spectra of **2**[Cl] (top) and **2**[OTf] (bottom) recorded in a Pyrex tube at −75 C using 1064 nm excitation. Symbols denote anion modes (*) as inferred by their absence from the spectrum of **2**[Cl] and an instrumental artifact (x).

triflate anion frequencies (marked by an asterisk) were assigned by comparison with a previous vibrational study[35] of this anion. The assignments were corroborated by comparing (Figure 3) the low-temperature Raman spectrum of the chloride salt **2**[Cl] with that of **2**[OTf].

The C-13 enriched (99 atom %) isotopomer of **1** (^{enr}**1**) was made via reduction of the enriched disulfide, $P_2Me_4S_2$ (^{enr}**5**), which was in turn prepared from $^{13}CH_3Br$ and $SPCl_3$ using procedures established for the natural abundance analogue.[36] Stepwise methylation of ^{enr}**1** with $^{13}CH_3$−OTf (i.e., C-13 enrichment of the CH_3 group only in CH_3OTf) yielded cations ^{enr}**2**$^{1+}$ and ^{enr}**3**$^{2+}$ with triflate counterions at natural abundance. The low-temperature Raman spectra of these isotopomers were obtained under identical conditions as their natural abundance analogues, permitting an unambiguous assignment of modes involving the carbon atoms. Selected data is compared in Table 2.

Spectral assignments were confirmed by comparison of experimental Raman frequencies, intensities, and isotopic shifts with values calculated for frameworks **1**, **2**$^{1+}$, and **3**$^{2+}$ in the gas phase. As a benchmarking exercise, the suitability of HF, MP2, and a variety hybrid DFT functionals was tested (Table 1)

Table 1. Experimental Raman and Calculated P−P Stretching Frequencies (cm^{-1}) for 1, 2^{1+}, and 3^{2+}[a]

compound	expt.	HF	MP2	B3LYP	PBE1PBE	B3PW91
1	455	488	477	436	459	449
2^{1+}	446	452	450	412	435	422
3^{2+}	456	457	442	412	428	420

[a]Experimental values for cations are for their triflate salts. The aug-cc-pVTZ basis set was used for all calculations.

using experimental values of the P−P stretching frequencies in **1**, **2**$^{1+}$, and **3**$^{2+}$, which fortuitously appears as the only peak in the P−P stretching region (400−500 cm^{-1} for single P−P bonds) of the spectra obtained for compounds **1**, **2**[OTf], **2**[Cl], and **3**$[OTf]_2$. The triflate counterions were omitted in calculations. While calculations carried out at the MP2 level provided the closest match with experimental values of ν(PP),

dx.doi.org/10.1021/ja507413s | J. Am. Chem. Soc. 2014, 136, 12498−12506

Table 2. Selected Experimental Raman Frequencies and Intensities (in parentheses) for the Natural Abundance and C-13 Enriched Isotopomers of 1, 2[OTf], and 3[OTf]$_2$[a]

	expt.			calcd			approximate mode assignments
	1	^{enr}**1**	Δ	**1**	^{enr}**1**	Δ	
P–P	455(57)	456(78)	1	459(10)	459(10)	0	$\nu(P_1P_2)$
P–C	666(53)	651(51)	15	677(29)	661(27)	16	$\nu(P_1C_{11}+P_1C_{12}+P_2C_{21}+P_2C_{22})$
	697(26)	683(26)	14	712(18)	699(17)	13	$\nu(P_1C_{11}+P_2C_{22}) - \nu(P_1C_{12}+P_2C_{21})$
	2[OTf]	^{enr}**2**[OTf]	Δ	$\mathbf{2}^{1+}$	$^{enr}\mathbf{2}^{1+}$	Δ	
P–P	446(32)	444(55)	2	435(13)	432(14)	3	$\nu(P_1P_2)$
P–C	668(12)	651(22)	17	672(3)	656(2)	16	$\nu(P_1C_{11}+P_1C_{12}) - \nu(P_2C_{21}+P_2C_{22}+P_2C_{23})$
	683(42)	666(64)	17	681(31)	664(29)	17	$\nu(P_1C_{11}+P_1C_{12}+P_2C_{21}+P_2C_{22}+P_2C_{23})$
	713(15)	699(27)	14	725(8)	710(7)	15	$\nu(P_1C_{11}) - \nu(P_1C_{12})$
	769(13)	n.o.	–	766(6)	752(5)	14	$\nu(P_2C_{22}) - \nu(P_2C_{21}+P_2C_{23})$
	773(12)	n.o.	–	773(5)	758(4)	15	$\nu(P_2C_{21}) - \nu(P_2C_{22})$
	3[OTf]$_2$	^{enr}3[OTf]$_2$	Δ	$\mathbf{3}^{2+}$	$^{enr}\mathbf{3}^{2+}$	Δ	
P–P	456(24)	452(34)	4	428(17)	425(18)	3	$\nu(P_1P_2)$
P–C	692(20)	675(14)	17	672(36)	656(32)	16	$\nu(P_1C_{11}+P_1C_{12}+P_1C_{23}+P_2C_{21}+P_2C_{22}+P_2C_{23})$
	784(17)	770(24)	14	766(9)	752(8)	14	$\nu(P_1C_{11}+P_1C_{13}+P_2C_{21}+P_2C_{23}) - \nu(P_1C_{12}+P_2C_{22})$

[a]Calculated Raman frequencies and intensities for the isotopomers of **1**, $\mathbf{2}^{1+}$, and $\mathbf{3}^{2+}$. Italics denote modes plotted in Figure 5. Expected modes that were not observed due to low intensity are denoted with the n.o. (not observed) label.

calculation of Raman intensities at this level with the aug-cc-pVTZ basis set was prohibitively memory intensive. HF level calculations were accurate at low frequencies but deviated significantly from experimental values at higher frequencies. Therefore, the PBE1PBE functional was chosen for calculating intensities, isotopic shifts, and visualizing atomic displacements.

As a representative example, Figure 4 shows spectra obtained for 3[OTf]$_2$ and ^{enr}3[OTf]$_2$. The ν(PP) frequencies (o) show

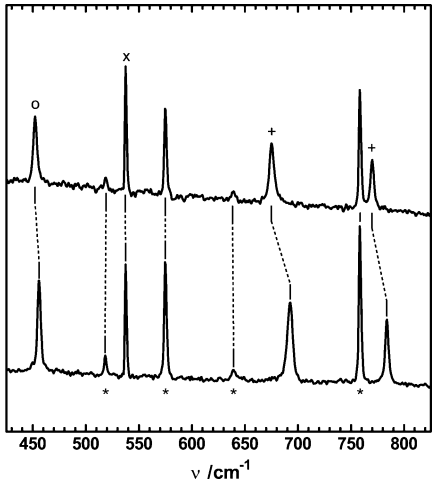

Figure 4. Raman spectra (425–825 cm^{-1}) of ^{enr}3[OTf]$_2$ (top) and 3[OTf]$_2$ (bottom) recorded in a Pyrex tube at −75 C using 1064 nm excitation. Symbols denote anion modes (*), the P–P stretching mode (o), the C–P stretching modes (+), and an instrumental artifact (x).

essentially minimal difference (max Δ = 3 cm^{-1}) between the isotopomers, consistent with this vibrational mode being decoupled from any of the P–C stretching modes. By comparison, the ν(EC) (E = P, H) modes show isotopic shifts of 11–16 cm^{-1}.

Neutral frameworks **4** and **5** contain one and two tetracoordinate phosphorus centers, respectively, and the cation in [P_2Me_5S][OTf] (**6**[OTf]) contains two tetracoordinate centers (Tables 3–5). The vibrational spectrum of **5** (Table 4) has been reported previously and assigned with the aid of isotopic enrichment.[37] Here we report the room-temperature, natural abundance infrared spectrum of **4** as a neat solid, with

Table 3. Selected Experimental and Calculated Infrared Frequencies for Natural Abundance P_2Me_4S (4)[a]

Labelling scheme		Expt.	Calcd.	Approximate mode assignments
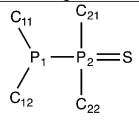	P-P	*423* (m)	418(5)	$\nu(P_1P_2)$
	P-C	586 (vs)	607(43)	$\nu(P_2C_{21}+P_2C_{22}+P_2S) - \nu(P_1P_2)$
		670 (w)	684(1)	$\nu(P_1C_{11}+P_1C_{12})$
		711 (m)	723(2)	$\nu(P_1C_{11}) - \nu(P_1C_{12})$
		722 (vs)	735(46)	$\nu(P_2C_{21}+P_2C_{22})$
		745 (m)	741(15)	$\nu(P_2C_{21}) - \nu(P_2C_{22})$

[a]Calculated intensities (km mol^{-1}) are given in parentheses. Italics denote modes plotted in Figure 5.

Table 4. Selected Experimental (ref 37) and Calculated Raman (R) or Infrared (IR) Frequencies for Natural Abundance $P_2Me_4S_2$ (5)[a]

Labelling scheme		Expt.	Calcd.	Approximate mode assignments
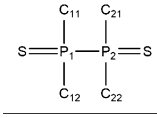	P-P	435 (R)	438 (R)	$\nu(P_1P_2)$
	P-C	730 (R)	750 (R)	$\nu(P_1C_{12}+P_2C_{22}) - \nu(P_1C_{11}+P_2C_{21})$
		733 (IR)	758 (IR)	$\nu(P_1C_{11}+P_2C_{22}) - \nu(P_1C_{12}+P_2C_{21})$
		743 (R)	760 (R)	$\nu(P_1C_{11}+P_1C_{12}+P_2C_{21}+P_2C_{22})$
		746 (IR)	765 (IR)	$\nu(P_1C_{11}+P_1C_{12}) - \nu(P_2C_{21}+P_2C_{22})$

[a]Experimental intensities were not reported. Italics denote modes plotted in Figure 5.

Table 5. Selected Experimental (ref 12) and Calculated Raman Frequencies for Natural Abundance P_2Me_5S (6^{1+})[a]

Labelling scheme		Expt.	Calcd.	Approximate mode assignments
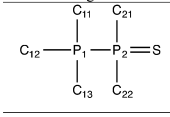	P-P	*442(30)*	415(19)	$\nu(P_1P_2)$
	P-C	591(28)	602(21)	$\nu(P_2C_{21}+P_2C_{22}+P_2S)$
		672(27)	672(26)	$\nu(P_1C_{11}+P_1C_{12}+P_1C_{13})$
		769(14)	745(8)	$\nu(P_2C_{21}) - \nu(P_2C_{22})$

[a]Normalized intensities are given in parentheses. Italics denote modes plotted in Figure 5.

dx.doi.org/10.1021/ja507413s | J. Am. Chem. Soc. 2014, 136, 12498–12506

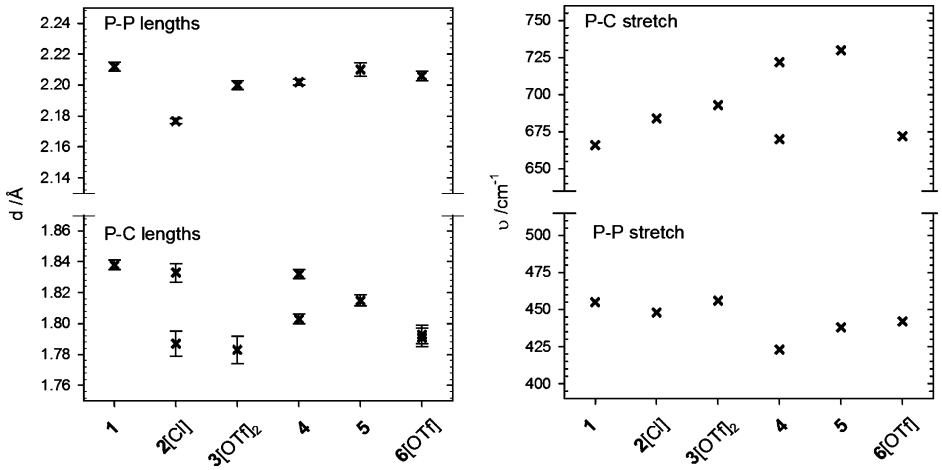

Figure 5. Left: Comparison of d(PP) and d(PC) in frameworks **1**−**6**. Error bars denote ±3 estimated standard deviations from the mean. Right: Comparison of ν(PP) and ν_{symm}(PC) in frameworks **1**−**6**.

select assignments derived from DFT calculations on a gas-phase model (Table 4).

Variations in the d(PE) and ν(PE) for E = P or C in frameworks **1**−**6** are illustrated in Figure 5, where the error bars denote the ±3 standard deviations for bond distances. The solid-state structure of compound **5** has been redetermined at 173.15 K and refined to a R1 value of 2.1%, since the reported structure (at 295 K, R1 = 8.9%) was found to have unacceptably large estimated standard deviations for using its metric parameters.[11] Two unique molecules are found in the unit cell, with statistically different P−P and P−C bond lengths. For clarity, the distance plotted in Figure 5 for this compound is an average from two independent molecules. Small and unsystematic variance (ca. 0.03 Å) in d(PP) is evident with changes in coordination number or charge at the phosphorus centers. Moreover there is no systematic correlation between d(PP) and the calculated homolytic or heterolytic bond dissociation energies. By comparison, while variation in d(PC) values is small, P−C bonds involving tetracoordinate centers are systematically, approximately 0.03 Å shorter than those involving tricoordinate phosphine centers, which are essentially equivalent to those in **1** (1.838 Å).[6] The P−C bonds at both tetracoordinate centers in **6**[OTf] are essentially identical to each other and are predictably shorter than the P−C bonds at the tricoordinate centers in **1**, **2**[OTf], and **4**. Values of d(PS) in **4** (1.970 Å)[10] and **5** (1.959 Å, average) are longer by ca. 0.05 Å than in **6**[OTf] (1.921 Å).[12]

Experimental values of ν(PP) exhibit the trend: **4** < **5** < $\mathbf{6}^{1+}$ < $\mathbf{2}^{1+}$ < $\mathbf{3}^{2+}$ ≈ **1**, but the differences are small (range = 33 cm^{-1}). Derivatives with a sulfur-substituted four-coordinate phosphorus center show ν(PP) frequencies that are slightly lower in energy than those in the corresponding cationic methylated analogues. Predictably, the ν(PP) wavenumber for $\mathbf{6}^{1+}$, which contains both sulfur and methyl substitution at a tetracoordinate phosphorus center, lies in between those for $\mathbf{3}^{2+}$ and **5**. Derivatives that contain both three and four coordinate phosphorus centers show lower ν(PP) frequencies than frameworks that contain only four coordinate centers. The effect is more pronounced in the sulfides (30 cm^{-1} variation) than the methylated cations (16 cm^{-1} variation). The results indicate that values of ν(PP) are more sensitive toward variation in the electronic and structural features of a PP-bonded compound than values of d(PP). Nevertheless there is no systematic correlation between values of ν(PP) and either the calculated homolytic or heterolytic dissociation energies, or values of d(PP).

Consistent with comparisons between the d(PP) and d(PC) values, the range of ν(PC) values is significantly greater than the range of ν(PP) values, as illustrated in Figure 5. For **4**, there is no vibrational mode that involves a symmetric and in-phase stretching of all PC bonds, and two frequencies, corresponding to discrete symmetric P−C stretches at P1 and at P2, are plotted. Similarly, for **6**, only the symmetric stretching mode involving the PMe_3 fragment is plotted since the mode involving the PMe_2S fragment shows strong coupling between the P−S and P−C stretches. Specific assigned P−C modes observed for compounds **1**, **2**[OTf], and **3**$[OTf]_2$ exhibit higher frequencies for frameworks with greater charge, correlated with shorter P−C bonds at the tetracoordinate centers relative to tricoordinate centers. The results evidence an inductive electron donation from the methyl groups to the tetracoordinate phosphorus centers, therefore the Coulombic destabilization intuitively expected for adjacent charges in $\mathbf{3}^{2+}$ is attenuated. Furthermore, all ν(PC) in **2**[OTf] or **3**$[OTf]_2$ occur at a higher wavenumber than the ν_{symm}(PC) in crystalline and gaseous PMe_3 (654 and 645 cm^{-1}, respectively).[38]

CONCLUSIONS

The established structural data and computational modeling of the P−P bond for a prototypical series of experimentally accessible tricoordinate-tricoordinate, tricoordinate-tetracoordinate, and tetracoordinate-tetracoordinate phosphorus−phosphorus bonding centers have been systematically analyzed and extended to provide a comprehensive data package. The assessment provides fundamental insights into the dissociation pathways for P−P bonds represented by Cases II−IV (Scheme 1) that may be broadly applicable to other homoatomic bonds.

The calculated P−P bond strengths for frameworks **1**−**6** show that, independent of molecular charge or coordination number of the phosphorus centers, homolytic bond dissociation is thermochemically favored over heterolytic bond dissociation. For $\mathbf{2}^{1+}$ and $\mathbf{6}^{1+}$, where heterolytic dissociation does not entail separation of opposite charges, the preference for homolytic dissociation is small. Semiempirical thermochemical cycles show that although, in the gas phase, the diphosphonium dication $\mathbf{3}^{2+}$ is comparable in energy to two

dx.doi.org/10.1021/ja507413s | J. Am. Chem. Soc. 2014, 136, 12498−12506

$[PMe_3]^+$ radical cations, it is the lattice enthalpy of $\mathbf{3}[OTf]_2$ in the solid state that enables isolation from a variety of reactions. The dramatic difference between the calculated stabilities of $\mathbf{3}^{2+}$ and $\mathbf{3}[OTf]_2$ is an arresting reminder that for cationic species, gas-phase stability calculations are poor guides for synthetic methods. The calculated P−P bond dissociation energies for frameworks **1** and $\mathbf{2}^{1+}$ show that the cationic charge strengthens the P−P bond such that it is comparable with the C−C bond in alkanes.

Infrared and low-temperature Raman spectra have been obtained for frameworks **1**−**6**, and the key stretching modes definitively assigned using isotopic enrichment and quantum chemical calculations. The P−P bond distances observed in these prototypical frameworks are independent of molecular charge or coordination number of the phosphorus centers, while the ν(PP) for bonds that involve a tetracoordinate phosphorus center are significantly lower than those involving only tricoordinate centers or only tetracoordinate centers. By comparison, the PC bond distances are distinctly shorter at quaternized phosphorus centers and correlate with higher ν_{symm}(PC) frequencies. Trends in values of d(PC) and ν_{symm}(PC) imply that a molecular cationic charge is distributed over the alkyl substituent. Importantly, there are no intuitive correlations between the experimentally observed bond distances or stretching frequencies and the calculated homolytic or heterolytic dissociation energies for these prototypical frameworks in the gas phase. We conclude that for the P−P bond, simple relationships or correlations between bond lengths, strengths, and force constants (e.g., Badger's rule, Gordy's rule)[39−42] are potentially misleading.

■ ASSOCIATED CONTENT

Supporting Information

Experimental details, Cartesian coordinates for computations, details of volume-based-thermodynamics, and vibrational spectroscopy data. This material is available free of charge via the Internet at http://pubs.acs.org.

■ AUTHOR INFORMATION

Corresponding Author

nburford@uvic.ca

Notes

The authors declare no competing financial interest.

■ ACKNOWLEDGMENTS

We thank Sivathmeehan Yogendra for experimental contributions and the Natural Sciences and Engineering Research Council (NSERC) of Canada and the Vanier Canada Graduate Scholarships Program for funding.

■ REFERENCES

(1) Wickham-Jones, C. T.; Moran, S.; Ellison, G. B. *J. Chem. Phys.* **1989**, *90*, 795−806.

(2) Scott, J. D.; Causely, G. C.; Russell, B. R. *J. Chem. Phys.* **1973**, *59*, 6577−6586.

(3) Haaland, A. *Angew. Chem., Int. Ed.* **1989**, *28*, 992−1007.

(4) Himmel, D.; Krossing, I.; Schnepf, A. *Angew. Chem., Int. Ed.* **2014**, *53*, 370−374.

(5) Frenking, G. *Angew. Chem., Int. Ed.* **2014**, *53*, 6040−6046.

(6) Mundt, O.; Riffel, H.; Becker, G.; Simon, A. *Z. Naturforsch., B* **1988**, *43*, 952−958.

(7) McAdam, A.; Beagley, B.; Hewitt, T. G. *Trans. Faraday Soc.* **1970**, *66*, 2732−2739.

(8) Chitnis, S. S.; MacDonald, E.; Burford, N.; Werner-Zwanziger, U.; McDonald, R. *Chem. Commun.* **2012**, *48*, 7359−7361.

(9) Weigand, J. J.; Riegel, S. D.; Burford, N.; Decken, A. *J. Am. Chem. Soc.* **2006**, *129*, 7969−7976.

(10) Gruber, M.; Jones, P. G.; Schmutzler, R. *Chem. Ber.* **1990**, *123*, 1313−1317.

(11) Lee, J. D.; Goodacre, G. W. *Acta. Crystallogr., Sect B* **1971**, *27*, 302−307.

(12) Weigand, J. J.; Burford, N.; Mahnke, D.; Decken, A. *Inorg. Chem.* **2007**, *46*, 7689−7691.

(13) Bews, J. R.; Glidewell, C. *J. Organomet. Chem.* **1983**, *255*, 49−60.

(14) Borisenko, K. B.; Rankin, D. W. H. *J. Chem. Soc., Dalton Trans.* **2002**, 3135−3141.

(15) Pietschnig, R. *J. Organomet. Chem.* **2007**, *692*, 3363−3369.

(16) Wolstenholme, D. J.; Weigand, J. J.; Davidson, R. J.; Pearson, J. K.; Cameron, T. S. *J. Phys. Chem. A* **2008**, *112*, 3424−3431.

(17) Gaussian 09 Suite was used for all calculations. See complete citation in Supporting Information. Test calculations with compound **1** showed that there was no significant difference in reaction energies calculated using the computationally-demanding diffuse aug-cc-pVTZ basis set and the smaller cc-pVTZ basis set. The MP2 method has been shown previously to accurately predict homolytic and heterolytic dissociation energies involving second and third period elements. See, for example: Boyd, S. L.; Boyd, R. J.; Bessonette, P. W.; Kerdraon, D. I.; Aucoin, N. T. *J. Am. Chem. Soc.* **1995**, *117*, 8816−8822. Boyd, R. J.; Mark Glover, J. N.; Pincock, J. A. *J. Am. Chem. Soc.* **1989**, *111*, 5152−5155. Boyd, S. L.; Boyd, R. J. *J. Am. Chem. Soc.* **1997**, *119*, 4214−4219.

(18) Hewertson, W.; Taylor, I. C. *J. Chem. Soc. C* **1970**, 1990−1992.

(19) Maaliki, C.; Lepetit, C.; Duhayon, C.; Canac, Y.; Chauvin, R. *Chem.—Eur. J.* **2012**, *18*, 16153−16160.

(20) Luo, Y. R. *Handbook of Bond Dissociation Energies in Organic Compounds*; CRC: Boca Raton, FL, 2003.

(21) Dyker, C. A.; Burford, N. *Chem.—Asian J.* **2008**, *3*, 28−36.

(22) Robertson, A. P. M.; Gray, P. A.; Burford, N. *Angew. Chem., Int. Ed.* **2014**, *53*, 6050−6069.

(23) Krossing, I.; Raabe, I. *Angew. Chem., Int. Ed.* **2004**, *43*, 2066−2090.

(24) Weigand, J. J.; Burford, N.; Decken, A.; Schulz, A. *Eur. J. Inorg. Chem.* **2007**, 4868−4872.

(25) Chitnis, S. S.; Carpenter, Y.; Burford, N.; McDonald, R.; Ferguson, M. J. *Angew. Chem., Int. Ed.* **2013**, *52*, 4863−4866.

(26) Robertson, A. P. M.; Burford, N.; McDonald, R.; Ferguson, M. J. *Angew. Chem., Int. Ed.* **2014**, *126*, 3548−3551.

(27) Jenkins, H. D. B.; Glasser, L. *J. Chem. Eng. Data* **2011**, *568*, 874−880.

(28) Gutowski, K. E.; Holbrey, J. D.; Rogers, R. D.; Dixon, D. A. *J. Phys. Chem. B* **2005**, *109*, 23196−23208.

(29) Shi, Q.; Tan, Z.; Di, Y.; Ti, B.; Li, Y.; Wang, S. *J. Chem. Eng. Data* **2007**, *52*, 941−947.

(30) 162 °C at 50 mmHg, corrected to 270 °C at 1 atm. *PHYSPROP Database*; Syracuse Research Corporation: Syracuse, NY, accessed on April 16th, 2014.

(31) Pan, X.; Chen, X.; Li, T.; Li, Y.; Wang, X. *J. Am. Chem. Soc.* **2013**, *135*, 34414−34417.

(32) Sasaki, S.; Sutoh, K.; Murakami, F.; Yoshifuji, M. *J. Am. Chem. Soc.* **2002**, *124*, 14830−14831.

(33) Nikitin, E. V.; Romakhin, A. S.; A Zaugmennov, V.; Babkin, Y. A. *Electrochim. Acta* **1997**, *42*, 2217−2224.

(34) Durig, J. R.; DiYorio, J. S. *Inorg. Chem.* **1969**, *8*, 2796−2802.

(35) (a) Johnston, D. H.; Shriver, D. F. *Inorg. Chem.* **1993**, *32*, 1045−1047. (b) Huang, W.; Frech, R.; Wheeler, R. A. *J. Phys. Chem.* **1994**, *98*, 100−110. (c) Miles, M. G.; Doyle, G.; Cooney, R. P.; Tobias, R. S. *Spectrochim. Acta* **1969**, *25A*, 1515−1526.

(36) Knackstedt, D. A., Investigation of Phosphenium Insertion into Phosphorus-Phosphorus Bonds, *M. Sc. Dissertation*, Dalhousie University: Halifax, NS, 2011.

(37) Durig, J. R.; Sens, M. A. *J. Cryst. Mol. Struct.* **1977**, *7*, 295−306.

(38) McKean, D. C.; McQuillan, G. P.; Murphy, W. F.; Zerbetto, F. *J. Phys. Chem.* **1990**, *94*, 4820−4831.

(39) Kaupp, M.; Riedel, S. *Inorg. Chim. Acta* **2004**, *357*, 1865−1872.
(40) Kaupp, M.; Schleyer, P. v. R. *J. Am. Chem. Soc.* **1993**, *115*, 1061−1073.
(41) Martell, J. M.; Boyd, R. J.; Shi, Z. *J. Phys. Chem.* **1993**, *97*, 7208−7215.
(42) Politzer, P.; Habibollahzadeh, D. *J. Chem. Phys.* **1993**, *98*, 7659−7660.